# **Quantitation of Trastuzumab and an Antibody to SARS-CoV-2 in Minutes Using Affinity Membranes in 96-Well Plates**

Hui Yin Tan<sup>1</sup>, Junyan Yang<sup>2</sup>, Jacqueline C. Linnes<sup>3</sup>, Christopher J. Welch<sup>4</sup>, and Merlin L. Bruening <sup>1,2\*</sup>

ABSTRACT: Quantitation of therapeutic monoclonal antibodies (mAbs) in human serum could ensure that patients have adequate levels of mAbs for effective treatment. This research describes the use of affinity, glass-fiber membranes in a 96-well-plate format for rapid (< 5 min) quantitation of the therapeutic mAb trastuzumab and a mAb against the SARS-CoV-2 spike protein. Adsorption of a poly(acrylic acid)-containing film in membrane pores and activation of the –COOH groups in the film enable covalent-linking of affinity peptides or proteins to the membrane. Passage of mAb-containing serum through the affinity membrane results in mAb capture within 1 min. Subsequent rinsing, binding of a secondary antibody conjugated to a fluorophore, and a second rinse yield mAb-concentration-dependent fluorescence intensities in the wells. Calibration curves established from analyses on different days have low variability and allow determination of mAb levels in separately prepared samples with an average error <10 %, although errors in single-replicate measurements may reach 30%. The assays can occur in diluted serum with physiologically relevant mAb concentrations, as well as in undiluted serum. Thus, the combination of 96-well plates containing affinity membranes, a microplate reader, and a simple vacuum manifold afford convenient mAb quantitation in <5 min.

## INTRODUCTION

This paper demonstrates selective and fast (<1 min) capture of monoclonal antibodies (mAbs) using 96-well plates containing glass-fiber membranes modified with a mimotope (a peptide that mimics an antibody epitope) or a SARS-CoV-2 antigen. Subsequent binding of fluorescently labeled secondary antibodies allows quantification of captured mAbs in minutes, even from undiluted serum. Thus, this research offers a simple, rapid method for immunoassays, which are fundamental analytical tools for clinical diagnostics, 1,2 food testing, 3,4 therapeutic drug monitoring, 5,6 and clinical pharmacokinetics studies for drug discovery. The global market for immunoassays was \$18 billion in 2018 and should grow due to increases in chronic and infectious diseases worldwide. 9

Immunoassays are ubiquitous, but they often require hours to complete.  $^{10\text{-}12}$  Enzyme-linked immunosorbent assays (ELISAs) are extremely successful and offer very low detection limits. For example, commercial kits have detections limits as low as 16 pg/mL for human TNF alpha  $^{10}$  and 8 pg/mL for human VEGF.  $^{11}$  However, these kits typically require at least 2 hours for analyses. Bead-based ELISAs and automated instrumentation enable such analyses in about 1 hour,  $^{13\text{-}15}$  although the techniques are labor intensive or require specialized instrumentation. He *et al.* recently developed miniaturized 96-well plates that require only 5  $\mu L$  of sample for each well and minimal equipment (a pipette and a magnet).  $^{16}$  ELISA using streptavidin beads in femtoliter-sized wells improves the limit of protein detection to sub-attomolar concentrations, but analysis times are still 2 hours.  $^{17}$ 

Determination of the concentration of therapeutic mAbs is important for the development and manufacturing of immunotherapeutic drugs, 18,19 and for monitoring the levels of these

mAbs in patients.<sup>20-22</sup> One challenge in mAb therapies is high patient-to-patient variability; the levels of mAbs in patients may differ four- to ten-fold between individuals at the same time after drug administration.<sup>20,23,24</sup> Low mAb concentrations lead to ineffective treatments, whereas high levels may cause side effects in some cases.<sup>20,22,25,26</sup> Hence, a rapid, inexpensive immunoassay could potentially enable better control of mAb dosing for maximized efficacy.

This paper describes assays developed for two model mAbs: trastuzumab and a mAb against SARS-CoV-2. Trastuzumab is a mAb that targets human epidermal growth factor receptor 2 (HER2) in tumors such as breast cancer, metastatic gastric cancer, and gastroesophageal junction adenocarcinoma. In clinical settings, trastuzumab has a trough concentration range of  $20-440~\mu g/mL$  in patient plasma with a desired value of  $>20~\mu g/mL$ . The variations in concentrations among patients depend on the number of metastatic sites, the concentration of HER2, and body weight. And 20 are 20 are 20 are 20 and 20 are 20 are 20 and 20 are 20 and 20 are 20 and 20 are 20 and 20 are 20 are 20 and 20 are 20 and 20 are 20 and 20 are 20 and 20 are 20 are 20 and 20 are 20 and 20 are 20 are 20 are 20 and 20 are 20 and 20 are 20 are 20 are 20 and 20 are 20 are 20 are 20 are 20 and 20 are 20 are 20 and 20 are 20 are 20 are 20 are 20 are 20 and 20 are 20 are 20 and 20 are 20 are 20 are 20 are 20 and 20 are 20 and 20 are 20 and 20 are 20 are

Like drugs for metastatic cancers, mAbs against coronavirus disease 2019 (COVID-19) could improve patient survival in this deadly pandemic. Despite the massive scale of the COVID-19 pandemic, the U. S. Food and Drug Administration (FDA) approved only a few therapeutic drugs under Emergency Use Authorization (EUA). These drugs include Remdesivir (an antiviral drug), 36-38 bamlanivimab/etesevimab (anti-SARS-CoV-2 mAbs), 39 and convalescent plasma, 40,41 which refers to transfusion of plasma collected from individuals who recovered from COVID-19 into recently infected COVID-19 patients. A rapid assay for SARS-CoV-2 antibodies would aid in selecting serum donors with high levels of antibodies for efficient treatment.

<sup>&</sup>lt;sup>1</sup>Department of Chemistry and Biochemistry, University of Notre Dame, Notre Dame, Indiana 46556, United States

<sup>&</sup>lt;sup>2</sup>Department of Chemical and Biomolecular Engineering, University of Notre Dame, Notre Dame, Indiana 46556, United States

<sup>&</sup>lt;sup>3</sup>Weldon School of Bioengineering, Purdue University, West Lafayette, IN 47907, United States

<sup>&</sup>lt;sup>4</sup>Indiana Consortium for Analytical Science & Engineering (ICASE), 410 W. 10th St., # 1020H, Indianapolis, IN 46202, United States

<sup>\*</sup>Corresponding author. mbruenin@nd.edu phone: +1 574-631-3024

Additionally, quantitative tests for antibodies against SARS-CoV-2 may be helpful in evaluating the immunity developed from a previous infection or vaccination to estimate the protection of an individual or community from the virus. Finally, assays for therapeutic mAbs used in COVID-19 treatment could prove useful in personalized dosing strategies.

Our group developed nylon membranes modified with peptide mimotopes for capture and analysis of mAbs using spin columns. 42,43 In general, membrane adsorbers are attractive for rapid capture of various molecules due to convection and short radial diffusion distances in micron-sized pores. 43,47 Adsorption of a poly(acrylic acid) (PAA)-containing film in membrane pores followed by activation of the film enables immobilization of affinity groups at high densities. 42,43,48,50 Modification of pores with either polymer brushes 45,47 or layer-by-layer films 43,51 can create affinity membranes with high binding capacities, and membrane modification using layer-by-layer deposition of a few polyelectrolyte layers is very convenient.

Flow through µm-sized pores combined with the high surface area to volume ratio in mimotope-modified membranes allows capture of antibodies within minutes. Moreover, the high mimotope density gives extensive mAb capture even with µM dissociation constants for mimotope-antibody complexes. Analysis of eluted mAbs using native tryptophan fluorescence occurred in 20 min using spin membranes. Esparately, our group reported the fabrication of nickel-containing membranes for rapid polyhistidine-tagged protein purification. Esparately, our group retionalized membranes allow convenient immobilization of polyhistidine-tagged proteins in an oriented fashion, which might be crucial for affinity binding of mAbs.

The present work advances membrane-based mAb analysis through the use of a fluorescent secondary antibody and glass-fiber membranes in 96-well plates. Using a vacuum manifold, flow of antibody-containing serum, rinsing solutions, and a secondary-antibody solution through a membrane can occur in around 3 min. Subsequent fluorescence detection on a plate reader completes the analysis in minutes. Such rapid and quantitative assays may prove useful for monitoring antibody levels during treatment, manufacturing, and research.

# **EXPERIMENTAL SECTION**

Materials. Glass-fiber membranes (Pall Corporation, A/C Glass Fiber 1 µm pores, 25 mm diameter, 254 µm thick) were cleaned in a UV/O3 chamber (Jelight, model 18) for 10 min prior to modification. AcroPrep Advance 96 Well plates (350 μL well volume, 1 μm pores) were acquired from Pall Corporation. The plates contain 660 µm-thick glass-fiber membranes at the bottom of 0.8-cm diameter wells. The Tra19 peptide (KGSGSGSQLGPYELWELSH) was synthesized GenScript with a purity greater than 95%. Poly(acrylic acid) (PAA, average molecular weight ~250,000 Da, 35% aqueous solution), polyethylenimine (PEI, branched, M<sub>w</sub> = 25,000 Da), N-(3-dimethylaminopropyl)-N'-ethylcarbodiimide hydrochloride (EDC), N-hydroxysuccinimide (NHS), Tween-20 surfactant, sodium phosphate monobasic monohydrate, sodium phosphate dibasic heptahydrate, sodium chloride, Nα,Nα-Bis(carboxymethyl)-L-lysine (aminobutyl NTA), imidazole, and human serum were purchased from Sigma-Aldrich. Deidentified patient serum samples were purchased from BioChemEd Services. Poly(vinyl) alcohol (PVA, 99-100 % hydrolyzed, approximate molecular weight 8600 Da) and nickel (II) sulfate hexahydrate were acquired from Acros Organics. Trastuzumab (Genentech) was used from its therapeutic formulation. Anti-SARS-CoV-2 Spike RBD (receptor binding domain) Antibody (Chimeric mAb, Human IgG1 (S1N-M130)) was purchased from AcroBiosystem and SARS-CoV-2 Spike RBD protein (his-tagged at the C-terminus, CHO-expressed) was purchased from GenScript. Goat Anti-Human IgG H&L (Cy5  $\circledR$ ) preadsorbed was acquired from Abcam. Buffers were prepared using analytical grade chemicals and deionized water (Milli-Q, 18.2 M $\Omega$  cm).

Immobilization of Tra19 in Porous Glass-Fiber Membranes in 96-well plates. The procedure for immobilization of a peptide mimotope in glass-fiber membranes includes modifying the membranes with a (PEI/PAA)<sub>2</sub> film, activating the -COOH groups of PAA, and allowing these groups to react with the free amine groups of Tra19. To deposit the first layer of PEI, 100 µL of 2 mg/mL branched PEI at pH 3 was added to the desired wells in a 96-well plate containing 1-µm-pore glass-fiber membranes. After a 5-min incubation, the solution was pulled through the membrane using a vacuum manifold. This procedure was repeated twice more with a fresh PEI solution to increase the PEI coverage, and the wells were washed with 1 mL of water with applied vacuum. Next, 100 µL of 1.1 mg/mL PAA in 0.5 M NaCl, pH 3 was added to each well, incubated for 5 min, and pulled through the membrane using vacuum. This PAA adsorption procedure was repeated twice more with a fresh solution to increase the coverage with PAA, and the wells were each washed with 1 mL of water. Additional PEI and PAA layers were deposited similarly.

Activation of the carboxylic acid groups of PAA to N-hydroxysuccinimidyl esters employed addition of 100 µL of 40 mM EDC, 40 mM NHS to each well, incubation for 10 min, and removal of the solution with vacuum. The procedure was repeated five more times with a fresh EDC/NHS solution and each well was then washed with 2 mL of water. Finally, 100 µL of 1.5 mg/mL Tra19 in water at pH 9 (pH adjusted with NaOH) was added to each well, incubated for 10 min, and pulled through the membrane. The Tra19 solution was recovered from the vacuum manifold trough and 100 µL was added back to each well for 10 min of incubation. (We observe loss of 10-20% of the solution after vacuum filtering. The recovered solution volume was compensated with more stock solution to give 100 μL for re-incubation). This incubating and passing of the Tra19 solution through the well were performed a total of six times. Finally, the wells were rinsed with 2 mL of water using vacuum. Crosslinking of the PEI/PAA films due to reaction of some of the amines of PEI with active esters likely increases film stability.

Immobilization of Tra19 in a 2 cm-Diameter Glass-Fiber **Membrane.** Using a membrane holder and a peristaltic pump, <sup>42</sup> 5 ml of 2 mg/mL branched PEI at pH 3 was circulated through the membrane for 15 min at 1 mL/min, and the membrane was washed with 10 mL of water. Subsequently 5 mL of 1.1 mg/mL PAA in 0.5 M NaCl, pH 3 was circulated through a 2 cm diameter glass-fiber membrane at 1 mL/min for 15 mins, followed by a 10-mL water wash. Then, another bilayer of PEI/PAA was deposited as described above. Activation of the membrane for Tra19 immobilization involved circulating 5 ml of 40 mM EDC, 40 mM NHS for 1 hour at 1 mL/min. After a 10-mL water rinse, 1 mL of 1 mg/mL Tra19 in pH 9 water (pH adjusted with NaOH) was circulated through the membrane for 1 hour at 1 mL/min. A final 10-mL water rinse was employed to remove unbound Tra19. The load, permeate, and washing solutions during Tra19 immobilization were collected, and the intrinsic tryptophan fluorescence of the peptide was measured using a Synergy H1 microplate reader by exciting at 280 nm and measuring emission from 300-400 nm, with peak emission at  $348 \pm 2$  nm. A calibration curve was established using standards of Tra19 at pH 9 to determine the Tra19 concentration in the load,

permeate, and washes. We diluted the permeate aliquots 20-fold with water prior to fluorescence measurements so absorbance due to liberated NHS would not interfere with the analyses.

To mimic the modification of membranes in 96-well plates, we also modified the 2-cm membranes using incubation, passage of the solution through the membrane at 5 mL/min using a peristaltic pump, and recycling of the Tra19 solutions for subsequent repeat incubations. This procedure employed the same incubation times and five-times the solution volumes used for the modifications of the 96-well plates. The increased volume approximately correlates with the higher surface area of the 2-cm membranes.

Breakthrough Curves in Tra19-modified Membranes. Using a peristaltic pump, a 2-cm diameter Tra19-modified membrane was rinsed with 5 mL of 20 mM phosphate buffer, pH 7.4 in 500 mM NaCl at 1 mL/min prior to passage of 5 mL of 100  $\mu$ g/mL trastuzumab (in the same buffer solution) through the membrane at a flow rate of 0.5 or 5 mL/min. Multiple fractions of permeate were collected in pre-weighed tubes and the permeate volume of each fraction was calculated based on mass. The concentrations of trastuzumab in the permeate fractions were determined using native fluorescence measured using a Synergy H1 microplate reader (excitation at 280 nm, emission at 330 nm± 2 nm) with a calibration curve based on trastuzumab standards in buffer.

Binding of Trastuzumab from Diluted Serum in 96-well Plates Containing Tra19-modified Membranes. With the vacuum running, each well was rinsed with 2 mL of wash buffer A (20 mM pH 7.4 phosphate buffer, 0.5 M NaCl, 0.1 % Tween-20), and then 0.5 mL of solution containing varied concentrations of trastuzumab  $(0-4 \mu g/mL)$  in 1% (v:v) human serum in 20 mM phosphate buffer (pH 7.4, 0.5 M NaCl) was loaded in each well. Subsequently, during vacuum filtration the plate was washed with 2 mL of wash buffer A in each well. One mL of 10 μg/mL secondary antibody (polyclonal anti-human IgG conjugated to Cy-5) in 20 mM phosphate buffer, pH 7.4, 0.5 M NaCl was then vacuum-filtered through each well, followed by 2 mL of wash buffer A. The concentration of mAb was determined by measuring the fluorescence of Cy5 bound to the well (excitation at 645 nm, emission at 670 nm) using a Synergy H1 Microplate Reader and comparing the fluorescence intensity to a calibration curve obtained using known concentrations of primary antibody in similar binding experiments.

Experiments followed the same protocol for pooled serum and individual patient sera. Because the pooled serum purchased from Sigma-Aldrich was heat-inactivated and filtered, the serum from individual patients was also heat-treated and filtered following established methods (Gemini Bio).<sup>52</sup>

Immobilization of RBD-his protein in Porous Glass-Fiber Membranes in 96-well plates. To capture an anti-spike antibody, we immobilized a polyhistidine-tagged form of the COVID-19 spike RBD protein (RBD-his) in membranes. The method for adsorption of polyelectrolyte layers in the membrane was the same as described above. After activation with EDC/NHS solution using the above procedure, 100 µL of 0.1 M aminobutyl NTA in a pH 10.5 solution (pH adjusted with NaOH) was added to the well and incubated for 10 min before removing the solution with vacuum. This step was repeated five more times using recycled solution. Then, 100 µL of 0.1 M nickel sulfate was added, incubated for 10 min, removed by vacuum, and this process was repeated five more times using recycled solution. To immobilize the RBD-his, 100 µL of 0.1 mg/mL RBD-his in 20 mM phosphate buffer, pH 7.4, 150 mM NaCl was incubated in each well for 10 min, vacuum filtered to recover the RBD-his solution, and the solution was re-applied

to each well for five more incubation and filtration steps. Finally, each well was washed with 2 mL of a pH 7.4 solution containing 20 mM phosphate buffer and 150 mM NaCl. Due to the high cost of the recombinant RBD-his, we did not quantify its immobilization.

Binding of anti-spike mAb in Diluted Serum to a RBD-hisfunctionalized 96-well Plate. With applied vacuum, the 96well plate was rinsed with 2 mL of wash buffer A and 0.5 mL of diluted serum spiked with different concentration of antispike mAb (0-10 µg/mL anti-spike in serum diluted with 20 mM pH 7.4 phosphate buffer containing 0.5 M NaCl, and 50 mM imidazole) was loaded into each well. This was followed by 1 mL of wash buffer B (20 mM pH 7.4 phosphate buffer in 0.5 M NaCl, 50 mM imidazole), 1 mL of wash buffer A, 0.5 mL of 20 μg/mL secondary antibody (polyclonal anti-human IgG conjugated to Cy-5) in pH 7.4 phosphate (20 mM) buffer containing 0.5 M NaCl, 1 mL of wash buffer B, and 1 mL of wash buffer A. Finally, the fluorescence of the secondary-antibodycontaining well (excitation at 645 nm and emission at 670 nm) was measured using a Synergy H1 microplate reader. A calibration curve was prepared using capture of the anti-spike mAb at different concentrations, binding of the labelled secondary antibody, and determination of the fluorescence intensity of Cy5 at 670 nm.

#### RESULTS AND DISCUSSION

The steps in the analytical procedure include modification of the membrane with affinity molecules, capture of a specific mAb, binding of a fluorescently labelled secondary antibody, and measurement of the well fluorescence (Figure 1). Thus, this section first describes Tra19 immobilization in glass-fiber membranes modified with adsorbed polyelectrolyte layers and examines the trastuzumab binding capacity in these modified membranes. Subsequently, using 96-well plates with mimotope-modified glass-fiber membranes, the research investigates the specific capture and detection of trastuzumab (spiked in human serum) in <5 min (including sample loading, washing, reagent binding, and fluorescence detection). Lastly, we assess the capture and quantification of a mAb against the SARS-COV-2 spike RBD protein. Those analyses employ a polyhistidine-tagged SARS-CoV-2 RBD protein immobilized in the membranes of 96-well plates.

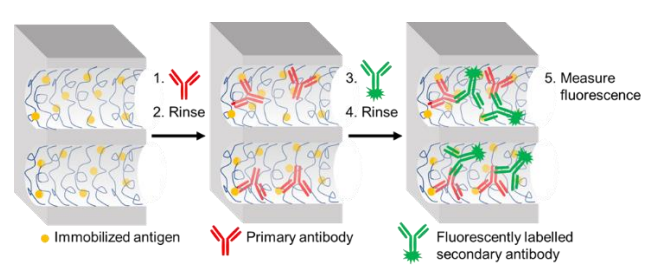


**Figure 1.** Scheme of a glass-fiber membrane modified with antigen, capture of a primary antibody of interest, and binding of a labelled secondary antibody to determine the primary antibody concentration using fluorescence.

Immobilization of Tra19 in Glass-Fiber Membranes. The first step in creating porous membranes to capture specific mAbs is immobilization of a selective affinity molecule in the pores. Mimotope peptides are attractive for binding mAbs because they are relatively small molecules, easy to immobilize, and highly specific.  $^{53-55}$  In prior work we immobilized  $25\pm4$  mg of the mimotope Tra19 per mL of a spongy nylon membrane.  $^{42}$  The immobilization method includes adsorption of a PAA-containing film, activation of the –COOH groups of PAA,

and reaction of primary amines on the mimotope, Tra19, with active esters. Continuous recirculation of solutions through 96-well plates is not feasible, so we add solutions to the wells and allow them to incubate for 5-10 min prior to vacuum filtration. Re-application of solutions to the wells multiple times mimics the continuous flow used previously.

To quantify Tra19 immobilization, we employed 2-cm-diameter glass-fiber membranes in a home-built holder using either continuous circulation of solutions or multiple incubations and filtrations with reuse of the effluent. The latter procedure is similar to that for modifying membranes in 96-well plates, but use of the 2-cm membranes and a peristaltic pump allows more quantitative collection of effluent solutions. Analysis of the Tra19 loading solution before and after multiple incubations and passes through the membrane suggests immobilization of  $2.9 \pm 0.5$  mg of Tra19 per mL of membrane. For comparison, the Tra19 binding capacity is  $5.1 \pm 1.3$  mg per mL when circulating solutions through the membrane. Thus, the incubation method results in approximately 40% less Tra19 immobilization. Regardless of the mimotope immobilization procedure, the mimotope concentration in glass-fiber membranes is nearly an order of magnitude less than that observed with nylon membranes, 42 presumably because of a lower surface area to volume ratio. Figure S1 in the supporting information presents SEM images of unmodified nylon and glass-fiber membranes (from wells), showing notable differences in porosity between the two substrates. The SEM images in Figure S1B and Figure 2A show that glass-fiber membranes have a wide distribution of pores sizes with strands of different thickness.

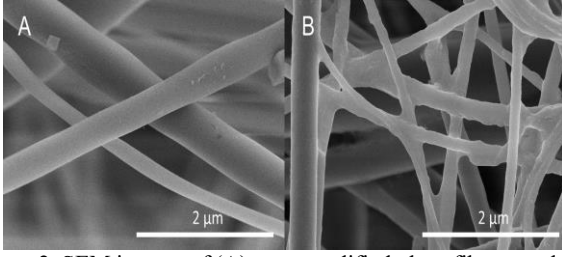


**Figure 2.** SEM images of (A) an unmodified glass-fiber membrane and (B) a (PEI/PAA)<sub>2</sub>-Tra19-modified glass-fiber membrane exposed sequentially to 4  $\mu$ g/mL Trastuzumab in 1 % human serum and fluorescently labelled secondary antibody, with rinsing between capture of each antibody. Membranes were removed from the well plate prior to sputter coating with 5 nm of gold/palladium and imaging using a Thermo Fisher Helios G4 Ux instrument.

Comparison of high-magnification SEM images of unmodified (Figure 2A) and Tra19-modified glass-fiber membranes (after antibody capture, Figure 2B) suggests an increase in surface roughness of the glass fibers after modification and antibody capture. Figure S2 of the supporting information shows other SEM images of unmodified and various modified glassfiber membranes. Previous studies showed that the thickness of (PEI/PAA)<sub>2</sub> and related films (deposited under conditions similar to this study) on flat substrates is <30 nm. 56-58 Modification with Tra19 and capture of antibodies might double the film thickness, but the total thickness of adsorbed material on a fiber should be at most 60 nm. However, in Figure 2B and Figure S2, there are areas where films appear thicker than expected. Immobilization of around 3 mg of Tra19 per mL of membrane suggests that the mimotope should occupy only 0.3% of the membrane volume and have minimal effect on membrane porosity, which is consistent with the images.

Quantifying Trastuzumab Capture in Tra19-modified Glass-Fiber Membranes. Subsequently we assessed the

binding of trastuzumab to 2-cm membranes containing the Tra19 mimotope. Figure 3 shows trastuzumab breakthrough curves during the passage of 50  $\mu$ g/mL or 100  $\mu$ g/mL trastuzumab solutions through different Tra19-modified glass-fiber membranes at two flow rates. For passage of the 100  $\mu$ g/mL solutions, the similar shapes of the curves obtained at 0.5 and 5 mL/min flowrates imply that capture is rapid compared to the residence time in the membrane. The shape of the curves may stem from the distribution of pore sizes in the membrane, where larger pores saturate first due to high flow rates and low surface area to volume ratios.

Using breakthrough curves, we determined the binding capacity by summing the products of aliquot volumes and the differences between the feed and permeate concentrations in each aliquot. The supporting information (Figure S3) shows replicate breakthrough curves with other membranes prepared using incubation or circulation. Breakthrough curves obtained with the  $100~\mu g/mL$  trastuzumab solution indicate capture of  $1.3\pm0.3$  mg of trastuzumab per mL of membrane; the breakthrough curves with a  $50~\mu g/mL$  solution show similar capacities. This is about eightfold less trastuzumab binding per volume than in nylon membranes that have higher surface area per volume.  $^{42}$  However, the thickness of the glass-fiber membrane in the 96-well plate is about five times the thickness of nylon membranes. Thus, for membranes with the same radius, the glass-fiber membranes should bind only 40% less trastuzumab.

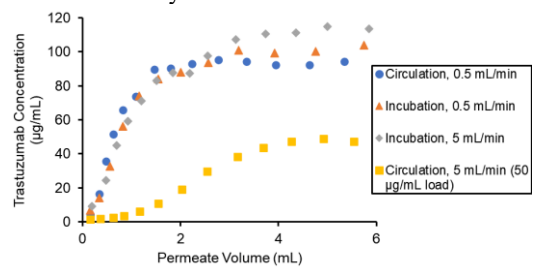


**Figure 3.** Concentrations of trastuzumab in the permeate passing through glass-fiber membranes modified using either circulation or serial incubations of polyelectrolyte, EDC/NHS and Tra19 solutions. 50 µg/mL or 100 µg/mL trastuzumab feed solutions were passed through the membrane at 0.5 or 5 mL/min. Blue circles – modification using circulation of solutions and flow of a 100 µg/mL trastuzumab solution through the membrane at 0.5 mL/min. Orange triangles - modification with serial incubations of solutions and flow of a 100 µg/mL trastuzumab solution through the membrane at 0.5 mL/min. Gray diamonds - modification with serial incubations of solutions and flow of a 100 µg/mL trastuzumab solution through the membrane at 5 mL/min. Yellow squares - modification using circulation of solutions and flow of a 50 µg/mL trastuzumab solution through the membrane at 5 mL/min.

Notably membranes modified with Tra19 using circulation of solutions show the same binding capacity as membranes modified by repeatedly incubating the membrane in solutions. The slightly lower amount of Tra19 immobilization with incubation does not significantly affect the trastuzumab binding. The molar ratio of bound trastuzumab to immobilized Tra19 is around 1:1500, so an increase in Tra19 density may simply result in additional mimotopes that are sterically inaccessible to antibodies.

The breakthrough curve at the lower feed concentration in Figure 3 (50  $\mu g/mL$ , yellow squares) shows capture of 80% of the trastuzumab in the first 2 mL of solution passed through the membrane and ~100% capture during passage of the first mL. The volume of the 2-cm diameter membrane in these studies is about 2.5 times that of the membrane in the 96-well plates. Thus, we estimate that the membranes in the well plates should

capture >80% of the mAb in the first 0.7 mL passed through the membrane, and experiments employed passage of 0.5 mL through a well. The capture percentage should increase further with lower concentrations if the affinity is high. Accordingly, we expect nearly quantitative capture of antibodies during passage of 0.5 mL of solution through a membrane in a well when antibody concentrations are <30  $\mu$ g/mL. Below we limit analyses to <30  $\mu$ g/mL, and more concentrated solutions will give signals outside the calibration range.

Modified 96-well Plates for Rapid Capture and Quantitation of Trastuzumab in Serum. We next investigated the capture of trastuzumab and a fluorescently labelled secondary antibody using Tra19-modified glass-fiber membranes in 96-well plates. Measurement of the captured secondary-antibody fluorescence as a function of trastuzumab concentration in the loading solution yields a calibration curve for determination of trastuzumab concentrations in human serum. In these experiments, we pass 0.5 mL of trastuzumab-spiked serum (undiluted or diluted 1:100) through Tra19-modified 96-well filter plates, wash with buffer, pass anti-human IgG conjugated to Cy5 through the plates, and perform a final wash before a fluorescence measurement (Figure 1). With a flow rate of ~5 mL/min obtained using a vacuum manifold, this entire procedure (including loading) requires only 3 min. Quantitation then occurs in <1 additional min using a microplate reader to detect the fluorescence from the captured secondary antibody. Figure 4 shows the resulting calibration curve for trastuzumab (0.01 - 4)µg/mL) spiked in 1% human serum. This concentration range approximately corresponds to the concentrations found in patients (0.2 – 4.4 µg/mL after a 1:100 dilution).<sup>30</sup> As expected, the fluorescence intensity increases with the concentration of trastuzumab spiked in the loading samples. The shape of the curve suggests that the secondary-antibody binding or fluorescence does not increase proportionally to the primary antibody binding at higher concentrations.<sup>59,60</sup> The fluorescence intensity increases when passing additional secondary antibody through the membrane, so we think that the nonlinear increase in signal appears because binding of Trastuzumab begins to saturate at high concentrations.

Although the relationship between fluorescence intensity from the well and the concentration of trastuzumab in the loading solution is non-linear, a 4-parameter logistic fit allows determination of trastuzumab concentration in serum. Note that the data show results from 60 different membranes (i.e. 60 wells) modified and examined on 3 different days, with no day-to-day correction. Thus, the data include well-to-well variability. For lot-to-lot variability in the plates, one would likely develop separate calibration curves for each lot. The coefficient of variation for the different points is at most 23%. The detection limit, where the signal is approximately 3 times the standard deviation of the blank plus the blank signal, is  $0.05~\mu g/mL$ .

We then used the calibration curve to determine trastuzumab concentrations in separately prepared spiked samples. As Figure S4 in the supporting information shows, the differences between the average determined concentrations (from 3 measurements) and the true concentrations are <10 %, even with the calibration curve and sample measurements taken on different days. Errors are larger in single replicates. This small error should be sufficient to determine if patient concentrations are above the 20  $\mu$ g/mL value (0.2  $\mu$ g/mL after dilution) needed for effective treatments. <sup>31,32,34</sup> Effective analysis occurs even with data obtained on different days. Thus, weekly calibration may be sufficient. Given the uncertainties in analyses at high concentrations, the assay might best serve in demonstrating that trasuzumab is above a threshold level.

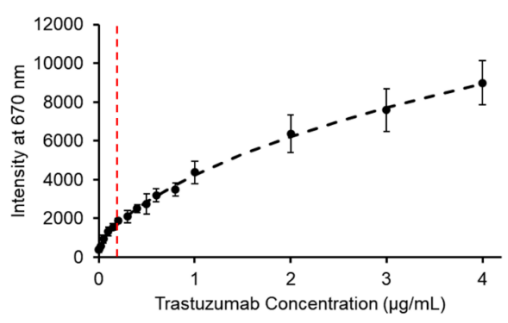


**Figure 4.** Calibration curve for analysis of trastuzumab spiked in 1% human serum. Analysis included capture of trastuzumab in a Tra19-modified 96-well plate, rinsing, binding of a fluorescently labelled secondary antibody, rinsing, and determination of the well fluorescence. The y-axis shows the fluorescence intensity of Cy5 (conjugated to the secondary antibody) at 670 nm. Error bars represent standard deviations from analyses with at least 3 replicate membranes. The dashed black curve is a 4-parameter logistic fit to the data. The red vertical line shows the lower limit needed to ensure effective therapies. Data show results from 60 different wells with analyses occurring on 3 different days.

The concentration of trastuzumab in undiluted serum (20-440) μg/mL) is outside of the calibration range in Figure 4 (0-4 μg/mL). Nevertheless, we are interested in examining whether mAb analysis is possible in the challenging matrix of undiluted serum. Thus, we loaded 0.5 mL of human serum containing 2 to 30 µg/mL of trastuzumab in wells containing Tra19-modified glass-fiber membranes and subsequently captured the Cy5-labelled secondary antibody. The resulting calibration curve in Figure 5 shows a clear response to trastuzumab in the undiluted serum and should allow determination of whether the trastuzumab level in a patient is above 10 µg/mL. However, the background signal (0 µg/mL trastuzumab) is 10-fold greater in undiluted serum than in 1% serum, so detection limits are much higher in undiluted serum. Unfortunately, at higher concentrations the trastuzumab-binding sites likely become saturated, so analysis of physiological concentrations is not possible without dilution.

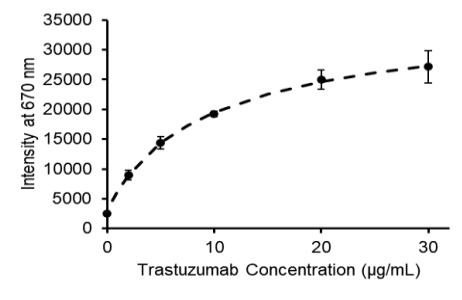


**Figure 5.** Calibration curve for analysis of trastuzumab spiked in undiluted pooled human serum. Analysis included capture of trastuzumab in a Tra19-modified 96-well plate, rinsing, binding of a fluorescently labelled secondary antibody, rinsing, and determination of the well fluorescence. Error bars show the standard deviations from 3 replicate experiments. The dashed curve is a 4-parameter logistic fit to the data. Data were obtained with 18 different wells, three different wells for each concentration, and analyses on multiple days.

We also examined the capture of trastuzumab from sera of individual patients instead of from the pooled serum purchased from Sigma-Aldrich. The individual sera came from 2 male and 2 female unidentified patients. Figure S5 shows that the Cy5 intensity at 670 nm again increases with the amount of trastuzumab added. Comparing the trastuzumab calibration

curve obtained with pooled serum and individual patient sera, the signal due to non-specific binding from serum alone (y-intercept in the calibration curves) increases ~2-fold in the individual patient sera. For data points obtained with various trastuzumab concentrations, we observe a ~1.5-fold increase in fluorescence intensity in individual patient sera samples compared to the pooled serum samples. The higher background binding from the individual patient sera could stem from different heat and filter treatment of the pooled serum versus the patient serum. Nevertheless, the calibration curve using data from all four individual patient sera shows a coefficient of variation <8 % at all spiked trastuzumab concentrations.

Selective Capture and Quantitation of an anti-spike mAb from Serum. We also explored the selective capture and quantitation of a mAb to the spike RBD protein of the SARS-CoV-2 virus. These analyses include immobilization of RBD protein in the 96-well glass-fiber plate and capture of a mAb (raised against the spike RBD protein). Initially, we attached the RBD protein to PAA-modified glass-fiber membranes via reaction of activated PAA with the primary amine groups in solvent-exposed lysine residues in the RBD protein. This method immobilizes the RBD protein in random orientations, likely making some of the binding sites of the RBD protein inaccessible to the antibody. To maximize the accessibility of RBD protein to the anti-spike mAb, we also immobilized this protein in a more oriented fashion using a polyhistidine tag at the RBD C-terminus. In this case, we first modify the membrane with NTA-nickel complexes<sup>51</sup> to capture the RBD-his.

For analysis of the anti-spike mAb concentration, we captured it in membranes containing RBD protein and subsequently bound the Cy5-labelled secondary antibody to generate a signal. Figure 6 shows the calibration curve for this analysis, which employed 96-well plates with immobilized RBD-his in glassfiber membranes. For comparison, Figure S6 shows the related calibration curve obtained with covalently immobilized RBD. The use of both types of immobilized RBD leads to fluorescence that increases with anti-spike mAb concentration, but the signal is 3 times higher when using the RBD-his. The detection limit is approximately 0.1 µg/mL (or 2 µg/mL before dilution). Typical analyses of "unknown" spiked samples show errors < 10 % for average concentrations (Figure S7), but errors are often larger in single-replicate measurements. Importantly, loading of the serum, rinsing, loading of the Cy5-labelled antibody, rinsing, and determination of fluorescence again requires <5 min.

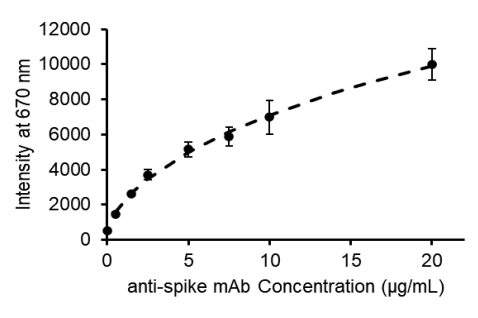


**Figure 6.** Calibration curve for the analysis of anti-spike mAb added to 5% pooled patient sera. Assays comprise binding of antispike mAb to an RBD-his-modified membrane in a 96-well plate, rinsing, binding of Cy5-labelled secondary antibody, rinsing, and measurement of fluorescence at 670 nm. Error bars represent the standard deviation from 3 replicate experiments. The dashed curve shows 4-parameter logistic fits to the data. Data were obtained with 24 different wells, three different wells for each concentration, and analyses on multiple days.

These analyses show the potential for monitoring a mAb-based COVID-19 therapy. Polyclonal donor antibodies will likely be more difficult to detect due to a range of affinities. Future work should examine detection of polyclonal antibodies to see if the technology could be useful for monitoring immunity. Such studies would need to determine the range of affinities over which the assay is effective as well as the dependence of signals on antibody affinity.

#### **CONCLUSIONS**

In this study, we successfully applied previous nylon-membrane-modification methods to glass-fiber membranes in 96well filter plates. Binding of Cy5-labelled secondary antibodies to captured mAbs in glass-fiber membranes allows determination of the primary mAb concentrations based on the fluorescence of Cy5. Using Tra19-modified 96-well plates, these assays have a trastuzumab analysis range that covers the clinical trough concentrations found in diluted patient serum. 30 Such assays can occur in both diluted and undiluted serum, although therapeutic trastuzumab concentrations in undiluted serum are outside the range of the technique. 96-well plates with immobilized RBD (part of the SARS-CoV-2 spike protein) allow determination of the concentration of an anti-spike mAb in diluted serum. Future studies with polyclonal spike protein antibodies are needed to examine the robustness of this method. Assays for both trastuzumab and the anti-spike mAb give average determined concentrations with an error < 10%, which is sufficient for many clinical purposes.<sup>20,61</sup>

#### ASSOCIATED CONTENT

## **Supporting Information**

The Supporting Information is available free of charge on the ACS Publications website.

Additional SEM images of membranes, additional breakthrough and calibration curves, plots of error in analyses, experimental procedures, and discussion of costs. (PDF)

## **AUTHOR INFORMATION**

## **Corresponding Author**

\* Merlin L. Bruening – Department of Chemical and Biomolecular Engineering, University of Notre Dame, Notre Dame, Indiana 46556, United States; orcid.org/ 0000-0002-4553-5143; Phone: +1 574-631-3024; Email: mbruenin@nd.edu

## **Author Contributions**

The manuscript was written through contributions of all authors. All authors have given approval to the final version of the manuscript.

#### ACKNOWLEDGMENT

The authors are grateful to the National Science Foundation (RAPID2031090) and the NSF IUCRC Center for Bioanalytical Metrology (1916601) for funding of this work. We thank Tatyana Orlova and Dr. Karl Cronberger from the University of Notre Dame for obtaining SEM images of our membranes. We are grateful to Brandy Verhalen (Corteva) and Ivan Budyak (Eli Lilly) for helpful suggestions and editing of this manuscript.

# REFERENCES

(1) Joung, H.-A.; Ballard, Z. S.; Ma, A.; Tseng, D. K.; Teshome, H.; Burakowski, S.; Garner, O. B.; Di Carlo, D.; Ozcan, A. Paper-

- Based Multiplexed Vertical Flow Assay for Point-of-Care Testing. *Lab Chip* **2019**, *19*, 1027–1034.
- (2) Clarke, O. J. R.; Goodall, B. L.; Hui, H. P.; Vats, N.; Brosseau, C. L. Development of a SERS-Based Rapid Vertical Flow Assay for Point-of-Care Diagnostics. *Anal. Chem.* **2017**, 89, 1405–1410.
- (3) Ramachandran, S.; Singhal, M.; McKenzie, K. G.; Osborn, J. L.; Arjyal, A.; Dongol, S.; Baker, S. G.; Basnyat, B.; Farrar, J.; Dolecek, C.; Domingo, G. J.; Yager, P.; Lutz, B. A Rapid, Multiplexed, High-Throughput Flow-through Membrane Immunoassay: A Convenient Alternative to ELISA. *Diagnostics* **2013**, *3*, 244–260.
- (4) Samsonova, J. V.; Safronova, V. A.; Osipov, A. P. Rapid Flowthrough Enzyme Immunoassay of Progesterone in Whole Cows' Milk. *Anal. Biochem.* **2018**, *545*, 43–48.
- (5) Broto, M.; McCabe, R.; Galve, R.; Marco, M.-P. A High Throughput Immunoassay for the Therapeutic Drug Monitoring of Tegafur. *Analyst* **2017**, *142*, 2404–2410.
- (6) Afonso, J.; de Sousa, H. T.; Rosa, I.; Carvalho, J.; Dias, C. C.; Magro, F. Therapeutic Drug Monitoring of CT-P13: A Comparison of Four Different Immunoassays. *Therap. Adv. Gastroenterol.* **2017**, *10*, 661–671.
- (7) Findlay, J. W.; Smith, W. C.; Lee, J. W.; Nordblom, G. D.; Das, I.; DeSilva, B. S.; Khan, M. N.; Bowsher, R. R. Validation of Immunoassays for Bioanalysis: A Pharmaceutical Industry Perspective. *J. Pharm. Biomed. Anal.* **2000**, *21*, 1249–1273.
- (8) Kitidee, K.; Nangola, S.; Hadpech, S.; Laopajon, W.; Kasinrerk, W.; Tayapiwatana, C. A Drug Discovery Platform: A Simplified Immunoassay for Analyzing HIV Protease Activity. *J. Virol. Methods* **2012**, *186*, 21–29.
- (9) Immunoassay market size & share report, 2021-2028 http://www.grandviewresearch.com/industry-analysis/immunoassay-market (accessed Dec 10, 2021).
- (10) Chen, Y.; Wu, D.; Sun, L. Clinical Significance of High-Mobility Group Box 1 Protein (HMGB1) and Nod-like Receptor Protein 3 (NLRP3) in Patients with Ulcerative Colitis. *Med. Sci. Monit.* **2020**, *26*, e919530.
- (11) Yi, X.; Chen, F.; Liu, F.; Peng, Q.; Li, Y.; Li, S.; Du, J.; Gao, Y.; Wang, Y. Comparative Separation Methods and Biological Characteristics of Human Placental and Umbilical Cord Mesenchymal Stem Cells in Serum-Free Culture Conditions. *Stem Cell Res. Ther.* **2020**, *11*, 183.
- (12) Oh, S.-H.; Choi, Y.-B.; Kim, J.-H.; Weihl, C. C.; Ju, J.-S. Quantification of Autophagy Flux Using LC3 ELISA. *Anal. Biochem.* **2017**, *530*, 57–67.
- (13) Campbell, J.; Pollock, N. R.; Sharon, A.; Sauer-Budge, A. F. Development of an Automated On-Chip Bead-Based ELISA Platform. *Anal. Methods* **2015**, *7*, 8472–8477.
- (14) Hand-Powered Centrifugal Microfluidic Disc with Magnetic Chitosan Bead-Based ELISA for Antibody Quantitation. *Sens. Actuators B Chem.* **2020**, *316*, 128003.
- (15) Calmo, R.; Chiadò, A.; Fiorilli, S.; Ricciardi, C. Advanced ELISA-like Biosensing Based on Ultralarge-Pore Silica Microbeads. *ACS Appl. Bio Mater.* **2020**, *3*, 5787–5795.
- (16) He, Z.; Huffman, J.; Curtin, K.; Garner, K. L.; Bowdridge, E. C.; Li, X.; Nurkiewicz, T. R.; Li, P. Composable Microfluidic Plates (CPlate): A Simple and Scalable Fluid Manipulation System for Multiplexed Enzyme-Linked Immunosorbent Assay (ELISA). *Anal. Chem.* **2021**, *93*, 1489–1497.
- (17) Kim, S. H.; Iwai, S.; Araki, S.; Sakakihara, S.; Iino, R.; Noji, H. Large-Scale Femtoliter Droplet Array for Digital Counting of Single Biomolecules. *Lab Chip* **2012**, *12*, 4986–4991.
- (18) Zschatzch, M.; Ritter, P.; Henseleit, A.; Wiehler, K.; Malik, S.; Bley, T.; Walther, T.; Boschke, E. Monitoring Bioactive and Total Antibody Concentrations for Continous Process Control by

- Surface Plasmon Resonance Spectroscopy. l.: Engineering in Life Sciences 2019, 19, 681–690.
- (19) Szmacinski, H.; Smith, D. S.; Hanson, M. A.; Kostov, Y.; Lakowicz, J. R.; Rao, G. A Novel Method for Monitoring Monoclonal Antibody Production during Cell Culture. *Biotechnol. Bioeng.* **2008**, *100*, 448–457.
- (20) Nugue, G.; Bidart, M.; Arlotto, M.; Mousseau, M.; Berger, F.; Pelletier, L. Monitoring Monoclonal Antibody Delivery in Oncology: The Example of Bevacizumab. *PLoS One* **2013**, *8*, e72021.
- (21) Damen, C. W. N.; de Groot, E. R.; Heij, M.; Boss, D. S.; Schellens, J. H. M.; Rosing, H.; Beijnen, J. H.; Aarden, L. A. Development and Validation of an Enzyme-Linked Immunosorbent Assay for the Quantification of Trastuzumab in Human Serum and Plasma. *Anal. Biochem.* **2009**, *391*, 114–120.
- (22) Imamura, C. K. Therapeutic Drug Monitoring of Monoclonal Antibodies: Applicability Based on Their Pharmacokinetic Properties. *Drug Metab. Pharmacokinet.* **2019**, *34*, 14–18.
- (23) Baselga, J.; Carbonell, X.; Castañeda-Soto, N.-J.; Clemens, M.; Green, M.; Harvey, V.; Morales, S.; Barton, C.; Ghahramani, P. Phase II Study of Efficacy, Safety, and Pharmacokinetics of Trastuzumab Monotherapy Administered on a 3-Weekly Schedule. *J. Clin. Oncol.* **2005**, *23*, 2162–2171.
- (24) Cobleigh, M. A.; Vogel, C. L.; Tripathy, D.; Robert, N. J.; Scholl, S.; Fehrenbacher, L.; Wolter, J. M.; Paton, V.; Shak, S.; Lieberman, G.; Slamon, D. J. Multinational Study of the Efficacy and Safety of Humanized Anti-HER2 Monoclonal Antibody in Women Who Have HER2-Overexpressing Metastatic Breast Cancer That Has Progressed after Chemotherapy for Metastatic Disease. *J. Clin. Oncol.* 1999, 17, 2639–2648.
- (25) Berinstein, N. L.; Grillo-López, A. J.; White, C. A.; Bence-Bruckler, I.; Maloney, D.; Czuczman, M.; Green, D.; Rosenberg, J.; McLaughlin, P.; Shen, D. Association of Serum Rituximab (IDEC–C2B8) Concentration and Anti-Tumor Response in the Treatment of Recurrent Low-Grade or Follicular Non-Hodgkin's Lymphoma. *Ann. Oncol.* **1998**, *9*, 995–1001.
- (26) Widmer, N.; Bardin, C.; Chatelut, E.; Paci, A.; Beijnen, J.; Levêque, D.; Veal, G.; Astier, A. Review of Therapeutic Drug Monitoring of Anticancer Drugs Part Two--Targeted Therapies. *Eur. J. Cancer* **2014**, *50*, 2020–2036.
- (27) Vu, T.; Claret, F. X. Trastuzumab: Updated Mechanisms of Action and Resistance in Breast Cancer. Front. Oncol. 2012, 2, 62.
- (28) Davidson, M.; Starling, N. Trastuzumab in the Management of Gastroesophageal Cancer: Patient Selection and Perspectives. *Onco. Targets. Ther.* **2016**, *9*, 7235–7245.
- (29) Gunturu, K. S.; Woo, Y.; Beaubier, N.; Remotti, H. E.; Saif, M. W. Gastric Cancer and Trastuzumab: First Biologic Therapy in Gastric Cancer. *Ther. Adv. Med. Oncol.* **2013**, *5*, 143–151.
- (30) Jamieson, D.; Cresti, N.; Verrill, M. W.; Boddy, A. V. Development and Validation of Cell-Based ELISA for the Quantification of Trastuzumab in Human Plasma. *J. Immunol. Methods* **2009**, *345*, 106–111.
- (31) De Santes, K.; Slamon, D.; Anderson, S. K.; Shepard, M.; Fendly, B.; Maneval, D.; Press, O. Radiolabeled Antibody Targeting of the HER-2/Neu Oncoprotein. *Cancer Res.* **1992**, *52*, 1916–1923.
- (32) Pegram, M.; Hsu, S.; Lewis, G.; Pietras, R.; Beryt, M.; Sliwkowski, M.; Coombs, D.; Baly, D.; Kabbinavar, F.; Slamon, D. Inhibitory Effects of Combinations of HER-2/Neu Antibody and Chemotherapeutic Agents Used for Treatment of Human Breast Cancers. *Oncogene* 1999, 18, 2241–2251.
- (33) Bruno, R.; Washington, C. B.; Lu, J.-F.; Lieberman, G.; Banken, L.; Klein, P. Population Pharmacokinetics of Trastuzumab in Patients with HER2+ Metastatic Breast Cancer. *Cancer Chemother. Pharmacol.* **2005**, *56*, 361–369.

- (34) Cosoon, V. F.; Ng, V. W.; Lehle, M.; Lum., B.L. Population Pharmacokinetics and Exposure-Response Analyses of Trastuzumab in Patients with Advanced Gastric or Gastroesophageal Junction Cancer. *Cancer Chemother. Pharmacol.* **2014**, *73*, 737–747.
- (35) Yang, J.; Zhao, H.; Garnett, C.; Rahman, A.; Gobburu, J. V.; Pierce, W.; Schechter, G.; Summers, J.; Keegan, P.; Booth, B.; Wang, Y. The Combination of Exposure-Response and Case-Control Analyses in Regulatory Decision Making. *J. Clin. Pharmacol.* **2013**, *53*, 160–166.
- (36) Beigel, J. H.; et al. ACTT-1 Study Group Members. Remdesivir for the Treatment of Covid-19 Final Report. *N. Engl. J. Med.* **2020**, *383*, 1813–1826.
- (37) Goldman, J. D.; et al. Remdesivir for 5 or 10 Days in Patients with Severe Covid-19. *N. Engl. J. Med.* **2020**, *383*, 1827–1837.
- (38) Spinner, C. D.; et al. Effect of Remdesivir vs Standard Care on Clinical Status at 11 Days in Patients with Moderate COVID-19: A Randomized Clinical Trial: A Randomized Clinical Trial. *JAMA* **2020**, *324*, 1048–1057.
- (39) Gottlieb, R. L.; et al. Effect of Bamlanivimab as Monotherapy or in Combination with Etesevimab on Viral Load in Patients with Mild to Moderate COVID-19: A Randomized Clinical Trial. *JAMA* **2021**, *325*, 632–644.
- (40) Joyner, M. J.; et al. Safety Update: COVID-19 Convalescent Plasma in 20,000 Hospitalized Patients. *Mayo Clin. Proc.* **2020**, *95*, 1888–1897.
- (41) Joyner, M. J.; et al. Effect of Convalescent Plasma on Mortality among Hospitalized Patients with COVID-19: Initial Three-Month Experience. medRxiv **2020**, 2020.08.12.20169359;
- (42) Liu, W.; Bennett, A. L.; Ning, W.; Tan, H.-Y.; Berwanger, J. D.; Zeng, X.; Bruening, M. L. Monoclonal Antibody Capture and Analysis Using Porous Membranes Containing Immobilized Peptide Mimotopes. *Anal. Chem.* **2018**, *90*, 12161–12167.
- (43) Berwanger, J. D.; Tan, H. Y.; Jokhadze, G.; Bruening, M. L. Determination of the Serum Concentrations of the Monoclonal Antibodies Bevacizumab, Rituximab, and Panitumumab Using Porous Membranes Containing Immobilized Peptide Mimotopes. *Anal. Chem.* **2021**, *93*, 7562–7570.
- (44) Schwark, S.; Sun, W.; Stute, J.; Lütkemeyer, D.; Ulbricht, M.; Sellergren, B. Monoclonal Antibody Capture from Cell Culture Supernatants Using Epitope Imprinted Macroporous Membranes. *RSC Adv.* **2016**, *6*, 53162–53169.
- (45) Chenette, H. C. S.; Welsh, J. M.; Husson, S. M. Affinity Membrane Adsorbers for Binding Arginine-Rich Proteins. *Sep. Sci. Technol.* **2017**, *52*, 276–286.
- (46) Wang, J.; Zhou, J.; Gowtham, Y. K.; Harcum, S. W.; Husson, S. M. Antibody Purification from CHO Cell Supernatant Using New Multimodal Membranes. *Biotechnol. Prog.* **2017**, *33*, 658–665.
- (47) Suresh, P.; Duval, C. E. Poly(Acid)-Functionalized Membranes to Sequester Uranium from Seawater. *Ind. Eng. Chem. Res.* **2020**, *59*, 12212–12222.
- (48) Bhattacharjee, S.; Dong, J.; Ma, Y.; Hovde, S.; Geiger, J. H.; Baker, G. L.; Bruening, M. L. Formation of High-Capacity Protein-Adsorbing Membranes through Simple Adsorption of Poly(Acrylic

- Acid)-Containing Films at Low PH. *Langmuir* **2012**, *28*, 6885–6892.
- (49) Bruening, M. L., Wijeratne, S., Ning, W., Dong, J., Liu, W. Polyacid-Functionalized Porous Membranes, Related Methods, and Related Polyacid Polymers. U.S. patent 2016073565A1, 2016.
- (50) Shang, Y.; Singh, P. R.; Chisti, M. M.; Mernaugh, R.; Zeng, X. Immobilization of a Human Epidermal Growth Factor Receptor 2 Mimotope-Derived Synthetic Peptide on Au and Its Potential Application for Detection of Herceptin in Human Serum by Quartz Crystal Microbalance. *Anal. Chem.* **2011**, *83*, 8928–8936.
- (51) Wijeratne, S.; Liu, W.; Dong, J.; Ning, W.; Ratnayake, N. D.; Walker, K. D.; Bruening, M. L. Layer-by-Layer Deposition with Polymers Containing Nitrilotriacetate, A Convenient Route to Fabricate Metal- and Protein-Binding Films. *ACS Appl. Mater. Interfaces* **2016**, *8*, 10164–10173.
- (52) Heat Inactivation of serum GeminiBio http://www.gembio.com/post/heat-inactivation-serum (accessed Dec 10, 2021).
- (53) Peltomaa, R.; Agudo-Maestro, I.; Más, V.; Barderas, R.; Benito-Peña, E.; Moreno-Bondi, M. C. Development and Comparison of Mimotope-Based Immunoassays for the Analysis of Fumonisin B1. *Anal. Bioanal. Chem.* **2019**, *411*, 6801–6811.
- (54) Chen, X.; Ding, X.; Zhu, L.; Zhang, G. The Identification of a B-Cell Epitope in Bovine Viral Diarrhea Virus (BVDV) Core Protein Based on a Mimotope Obtained from a Phage-Displayed Peptide Library. *Int. J. Biol. Macromol.* **2021**, *183*, 2376–2386.
- (55) Shi, W.; Zhao, L.; Xu, Y.; Xu, G.; Zeng, Y. Identification of Mimotope of Mycoplasma Pneumoniae P1 Protein and Its Potential Value in Serodiagnosis. *Biotechnol. Biotechnol. Equip.* **2019**, *33*, 1034–1041.
- (56) Shiratori, S. S.; Rubner, M. F. pH-Dependent Thickness Behavior of Sequentially Adsorbed Layers of Weak Polyelectrolytes. *Macromolecules* **2000**, *33*, 4213–4219.
- (57) Yang, Y.-H.; Haile, M.; Park, Y. T.; Malek, F. A.; Grunlan, J. C. Super Gas Barrier of All-Polymer Multilayer Thin Films. *Macromolecules* **2011**, *44*, 1450–1459.
- (58) Ma, Y.; Dong, J.; Bhattacharjee, S.; Wijeratne, S.; Bruening, M. L.; Baker, G. L. Increased Protein Sorption in Poly(Acrylic Acid)-Containing Films through Incorporation of Comb-like Polymers and Film Adsorption at Low pH and High Ionic Strength. *Langmuir* **2013**, *29*, 2946–2954.
- (59) Gao, Z.-Y.; Zhang, Q.-L.; Shi, C.; Gou, J.-X.; Gao, D.; Wang, H.-B.; Yao, S.-J.; Lin, D.-Q. Antibody Capture with Twin-Column Continuous Chromatography: Effects of Residence Time, Protein Concentration and Resin. Sep. Purif. Technol. 2020, 253, 117554.
- (60) Feidl; Garbellini; Luna; Vogg; Souquet; Broly; Morbidelli; Butté. Combining Mechanistic Modeling and Raman Spectroscopy for Monitoring Antibody Chromatographic Purification. *Processes* **2019**, *7*, 683.
- (61) McBride, J. M.; Lim, J. J.; Burgess, T.; Deng, R.; Derby, M. A.; Maia, M.; Horn, P.; Siddiqui, O.; Sheinson, D.; Chen-Harris, H.; Newton, E. M.; Fillos, D.; Nazzal, D.; Rosenberger, C. M.; Ohlson, M. B.; Lambkin-Williams, R.; Fathi, H.; Harris, J. M.; Tavel, J. A. Phase 2 Randomized Trial of the Safety and Efficacy of MHAA4549A, a Broadly Neutralizing Monoclonal Antibody, in a Human Influenza A Virus Challenge Model. *Antimicrob. Agents Chemother.* **2017**, *61*, 01154-17.

